An externally accessible linker region in the sodium-coupled phosphate transporter PiT-1 (SLC20A1) is important for transport function

Ravera, Silvia ; Murer, Heini ; Forster, Ian C

Abstract: Background/Aims : Members of the SLC20 cotransporter family (PiT-1, PiT-2) are ubiquitously expressed in mammalian tissue and are thought to perform housekeeping functions for intracellular Pi homeostasis as well as being implicated in vascular calcification and renal Pi reabsorption. The aims of this study were to investigate the topology of a linker region in PiT-1 between the predicted 2(nd) and 3(rd) transmembrane domains and to investigate the functional consequences of cysteine substitutions in this region. Methods : Cysteines were substituted at 18 sites in the Xenopus PiT-1 isoform and the mutants were expressed in Xenopus laevis oocytes. Transport function of the mutants was investigated by (32)P tracer or two electrode voltage clamp before and after thiol modification of the novel Cys. Results : Exposure to the thiol reactive reagent resulted in diminished transport function for 7 mutants. The apparent accessibility of 5 of the mutated sites, estimated from the rate of functional thiol modification, was site-dependent. Cysteine substitution at some sites also altered the apparent affinity for Pi and cation (Na(+)/Li(+)) and substrate (phosphate/arsenate) selectivity, further underscoring the importance of this linker in defining PiT-1 transport characteristics. Conclusions: The external accessibility of a linker in PiT-1 was confirmed and sites were identified that determine substrate selectivity and transport function.

DOI: https://doi.org/10.1159/000350135

Cellular Physiology and Biochemistry

Cell Physiol Biochem 2013;32:187-199
DOI: 10.1159/000350135
Published online: July 18, 2013
Accepted: July 01, 2013

1421-9778/13/0321-0187$38.00/0

Original Paper

An Externally Accessible Linker Region in the Sodium-Coupled Phosphate Transporter PiT-1 (SLC20A1) is Important for Transport Function

Silvia Ravera Heini Murer Ian C. Forster

Institute of Physiology and Center for Integrative Human Physiology (ZIHP), University of Zurich, Zurich, Switzerland

Key Words
Na^+/P_i cotransport • Two-electrode voltage clamp • SLC20 • Cysteine scanning

Abstract
Background/Aims*:** Members of the SLC20 cotransporter family (PiT-1, PiT-2) are ubiquitously expressed in mammalian tissue and are thought to perform housekeeping functions for intracellular P_i homeostasis as well as being implicated in vascular calcification and renal P_i reabsorption. The aims of this study were to investigate the topology of a linker region in PiT-1 between the predicted 2nd and 3rd transmembrane domains and to investigate the functional consequences of cysteine substitutions in this region. ***Methods*:** Cysteines were substituted at 18 sites in the *Xenopus* PiT-1 isoform and the mutants were expressed in *Xenopus laevis* oocytes. Transport function of the mutants was investigated by ^{32}P tracer or two electrode voltage clamp before and after thiol modification of the novel Cys. ***Results*:** Exposure to the thiol reactive reagent resulted in diminished transport function for 7 mutants. The apparent accessibility of 5 of the mutated sites, estimated from the rate of functional thiol modification, was site-dependent. Cysteine substitution at some sites also altered the apparent affinity for P_i and cation (Na^+/Li^+) and substrate (phosphate/arsenate) selectivity, further underscoring the importance of this linker in defining PiT-1 transport characteristics. ***Conclusions: The external accessibility of a linker in PiT-1 was confirmed and sites were identified that determine substrate selectivity and transport function.

Ian C. Forster, PhD

Institute of Physiology, University of Zurich,
Winterthurerstrasse 190, CH-8057 Zurich (Switzerland)
Tel. +41 (0)44 635 5059, Fax +41 (0) 44 635 6814, E-Mail Iforster@access.uzh.ch

Introduction

Symporters belonging to two distinct solute carrier gene families (SLC20 and SLC34) mediate Na^+-coupled transport of inorganic phosphate (P_i) in mammals. The gene products of the SLC34 family (NaPi-IIa, NaPi-IIb and NaPi-IIc) are responsible for P_i absorption and reabsorption across the apical membranes of many epithelia, including kidney and small intestine, where they play essential roles in P_i homeostasis (for review see [1-4]). Their transport properties have been extensively characterized by heterologous expression in *Xenopus* oocytes and a number of structure-function studies based on cysteine scanning and voltage-clamp fluorometry have been described (reviewed in [3]). The gene products of the SLC20 family (SLC20A1 or PiT-1and SLC20A2 or PiT-2, also referred to as type III Na^+/P_i transporters) were initially identified as retroviral receptors and later shown to be Na^+-coupled P_i cotransporters [5-7]. In humans they have a broad tissue distribution at the RNA level [8] and are considered to be ubiquitously expressed, which suggested that they play a housekeeping role for P_i homeostasis in cells. However, specific roles for SLC20 proteins have been reported: for example, P_i transport mediated by PiT-1 most likely plays a role in providing P_i for the formation of mineralized bone [9-11], PiT-1 has been strongly implicated in calcification of vascular tissue in response to hyperphosphatemia [12-17] and a transport-independent role for PiT-1 in the regulation of TNF-induced apoptosis was reported [18]. Importantly, PiT-2 has been localized to the apical membrane of renal proximal tubule cells in the mammalian kidney and displays a different regulatory response from the SLC34 family members to changes in dietary P_i [19, 20], although its precise role in renal P_i handling is yet to be fully elucidated [21]. Most recently, a role for PiT-2 in the CNS has been identified, whereby mutations in human PiT-2 (SLC20A2) have been implicated in familial idiopathic basal ganglia calcification (Fahr's disease) [22, 23].

An important functional distinction between SLC34 and SLC20 proteins is that the former preferentially transport divalent phosphate (HPO_4^{2-}), whereas it is established that SLC20 proteins prefer monovalent phosphate ($H_2PO_4^-$) [19, 24, 25]. Kinetic analyses of SLC20 proteins have revealed other functional differences such as pH sensitivity, substrate specificity and driving cations [19, 26-28], thereby underscoring the potential for different functional roles in the physiological context.

Like SLC34 proteins, no 3-D structural information is currently available for the SLC20 family members, however unlike the former, only limited structure-function studies have been performed on these transporters [26, 29-32]. The secondary topology is predicted to contain 12 transmembrane domains with extracellularly orientated N- and C-termini [32-35] (Fig. 1A) and some critical regions and sites important for the viral recognition function have also been identified [29, 30, 32, 36]. In addition, two studies have identified sites critical for transport function [29, 37].

The current lack of detailed structure-function information specifically relating to SLC20 proteins as Na^+/P_i cotransporters prompted us to start with a systematic application of the substituted cysteine accessibility method (SCAM) [38] to one region of the PiT-1 protein that was shown to contain functionally important sites [31]. Based on topology predictions, this region should be at least partly accessible to the external medium (Fig. 1B). Our findings confirm this prediction and we suggest that this region may play an important role in substrate coordination and selectivity.

Materials and Methods

Molecular Biology and oocyte expression

cDNAs encoding *Xenopus laevis* PiT-1 (XlPiT-1) from RZPD (German Resource Center for Genome Research) were subcloned into a KSM expression vector [39] to improve expression in *Xenopus laevis* oocytes. The plasmid was linearized and used as a template for the synthesis of capped cRNA using the T3 Message Machine kit (Ambion, Austin, TX, USA). Novel cysteines were introduced using the Quickchange

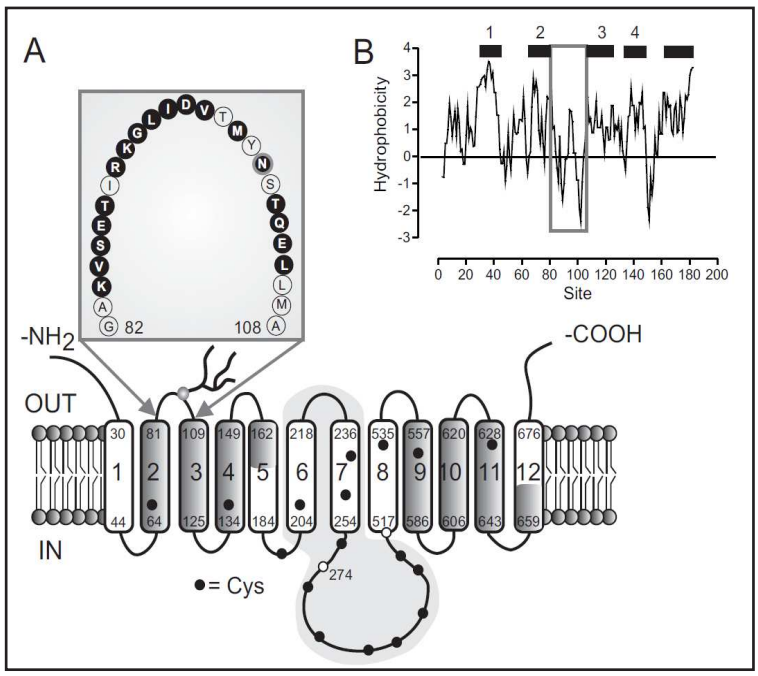

Fig. 1. Topology of PiT-1. A) Secondary topology of PiT-1 showing predicted transmembrane domains (TMDs) (numbered 1-12) and linker region between TMD2 and TMD3 where cysteine substitutions were made (inset). Shaded TMDs are PD1131 homology domains predicted to play an important role in transport function [32, 35]. In PiT-2, deletion of the light grey shaded region (L202-V517) encompassing the large intracellular loop and TMD 6, 7 results in impaired transport function and loss of retroviral function [32], whereas deletion of the region P274-V517 results in loss of retroviral function only [32]. Approximate positions of the 17 native Cys residues for XlPiT-1 are indicated (filled circles). Inset : sites mutated to cysteines (filled circles) and location of a predicted N-glycosylation site (grey outlined circle). Sites in PiT-2 (SLC20A2), corresponding to Glu-87 and Asp-95 were identified by Bøttger and Pedersen to be important for transport function [31].B) Hydrophobicity plot for the region up to the end of TMD5 (Protscale, according to Kyte-Doolittle hydrophobicity scale) [49]. Boxed region represents linker under investigation. Filled boxes: predicted TMDs. All numbering refers to XlPiT-1 sequence.

site-directed mutagenesis kit (Stratagene Inc., La Jolla, CA, USA). The sequence was verified by sequencing (Microsynth, Switzerland), linearized with *NotI* and cRNA was synthesized in the presence of Cap analog using the T7 Message Machine kit (Ambion, Inc., Austin, TX, USA). Stage V-VI defolliculated oocytes from *Xenopus laevis* were isolated and maintained as described previously [40]. Oocytes were injected with 50 nl of cRNA (50 ng). Control oocytes were either injected with 50 nl of water or not injected. Oocytes were incubated at 16°C in modified Barth's solution, containing (in mM) 88 NaCl, 1 KC1, 0.41 $CaCl_2$, 0.82 $MgSO_4$, 2.5 $NaHCO_3$, 2 $Ca(NO_3)_2$, 7.5 HEPES, pH 7.4 adjusted with TRIS. The solution was supplemented with 5 mg/l doxycyclin.

Electrophysiology and radiotracer flux experiments were performed 2–5 days after injection. Each data set was obtained from at least two batches of oocytes from two different frogs.

Reagents and solutions

All standard reagents were obtained from either Sigma-Aldrich or Fluka (Buchs, Switzerland). 2-(trimethylammonium) ethylmethanethiosulfonate bromide (MTSET) was obtained from Toronto Research Chemicals. The solution compositions were as follows: Control superfusate (100Na) (in mM): 100 NaCl, 2 KCl, 1.8 $CaCl_2$, 1 $MgCl_2$, 10 HEPES, adjusted to pH 7.4 using TRIS. Choline solution (100Ch): as for 100Na with isosmotic substitution of 100 choline chloride. Lithium superfusate (100Li): as for 100Na with isosmotic substitution of LiCl. Substrate test solutions: P_i was added from 1 M K_2HPO_4 and KH_2PO_4 stocks premixed to give the required pH (7.4). A similar procedure was used for arsenate.

Radiotracer uptake

Groups of oocytes (7–10 oocytes/group) were first allowed to equilibrate in uptake solution without tracer. After aspiration of this solution we added 100 µl uptake solution containing radiotracer (^{32}P) (Perkin Elmer, Switzerland). The uptake was allowed to proceed for 15–20 min before it was stopped by washing the oocytes 4 times with 4 ml ice-cold 100Ch solution containing 0.5 mM cold P_i. Uptake of $^{32}P_i$ alone was

carried out using 100Na solution and 1 mM cold P_i, to which $^{32}P_i$ (specific activity 10-20 mCi/ mmol P_i) was added. After washing, oocytes were placed individually in a scintillation vial and lysed in 250 µl 10% SDS. $^{32}P_i$ activities of individual oocytes were counted using a Packard Tri-Carb 2900TR scintillation counter.

Electrophysiology

Standard two-electrode voltage clamp hardware was used (GeneClamp, Model 500, Molecular Devices), or a laboratory-built clamp [41]. The voltage clamp hardware was controlled, and data were acquired, using pClamp 8-9 software (Molecular Devices), which also controlled valves for solution switching. At the onset of each experiment the oocyte was clamped to a holding potential (V_h) = -50 mV and superfused with 100Na solution. To measure P_i-induced currents (I_{P_i}), the superfusate was switched to one containing P_i and the change in the holding current was monitored. When the current reached a steady-state data were acquired and the perfusate was switched back and washout of P_i was monitored by observing the return of holding current to baseline.

Determination of apparent P_i affinity

To determine the apparent affinity constant for P_i ($K_{0.5}^{P_i}$) the electrogenic response to different P_i concentrations added to the 100Na control solution was measured at a defined membrane potential. Oocytes were voltage-clamped to V_h = -60 mV and voltage steps were applied in the range -160 to +60 mV for typically 100 ms. To measure P_i-induced currents (I_{P_i}), the superfusate was switched from the control (100Na) solution to one containing a given concentration of P_i and when the holding current had reached a steady-state, the voltage steps were repeated. The control data set was subtracted from the data set obtained in the presence of P_i to give I_{P_i} for each [P_i] and test voltage. To control for response rundown (e.g.[19]), each P_i test application or the complete series was bracketed by a 1 mM P_i measurement, which was used to correct the preceding data sets if necessary. Estimates of $K_{0.5}^{P_i}$ were obtained by fitting data with a form of the Michaelis-Menten equation given by:

$$I_{P_i} = I_{P_i}^{max} [P_i] / ([P_i] + K_{0.5}^{P_i}) + I_{OFF} \quad (1)$$

where $I_{P_i}^{max}$ is the maximum current attainable, I_{OFF} is a variable offset to account for reversal I_{P_i} at low [P_i]. To account for the differences in expression levels between individual oocytes, data obtained from each oocyte were normalized to I_{P_i} recorded at -100 mV with 100Na and 1 mM P_i before fitting the data with Eqn. 1.

Thiol modification by MTS reagents

MTSET was prepared in a 1 M stock solution (water or DMSO), which was kept at -20°C until required and further diluted with water or DMSO to give 1000-fold concentrated experimental aliquots before adding to the 100Na superfusate to achieve the final concentration as indicated. For ^{32}P uptake assays, oocytes were incubated in MTSET for 5 min and washed for 1 min. For electrophysiology, MTSET was applied to the recording chamber by gravity feed via a 0.5-mm-diameter cannula positioned near the cell. To determine the apparent accessibility, MTSET at a predetermined concentration was applied for 1 min followed by washout. During incubation, oocytes were clamped at V_h= -50 mV. After washout I_{P_i} in response to 1 mM P_i at V_h =-50 mV was again measured and the MTSET application was repeated. The fixed MTSET concentrations were chosen by pretesting to facilitate determination of the modification rate so that degradation of MTS reagent was minimised. The P_i response remaining after each successive application of MTS reagent was measured and plotted as a function of the cumulative exposure time, normalized to the initial I_{P_i}. The data were fit with a single decaying exponential to determine the effective second order reaction constant using an equation of the form:

$$I_{P_i}^{t} = (I_{P_i}^{0} - I_{P_i}^{\infty}) \exp(-t[MTS]k^*) + I_{P_i}^{\infty} \quad (2)$$

where $I_{P_i}^{t}$ is the P_i-induced current after a cumulative exposure time t, $I_{P_i}^{0}$ is the initial P_i-induced current, $I_{P_i}^{\infty}$ is the P_i-induced current at infinity, [MTS] is the concentration of MTS reagent (assumed to be in excess) and k^* is the effective second order rate constant e.g. [38].

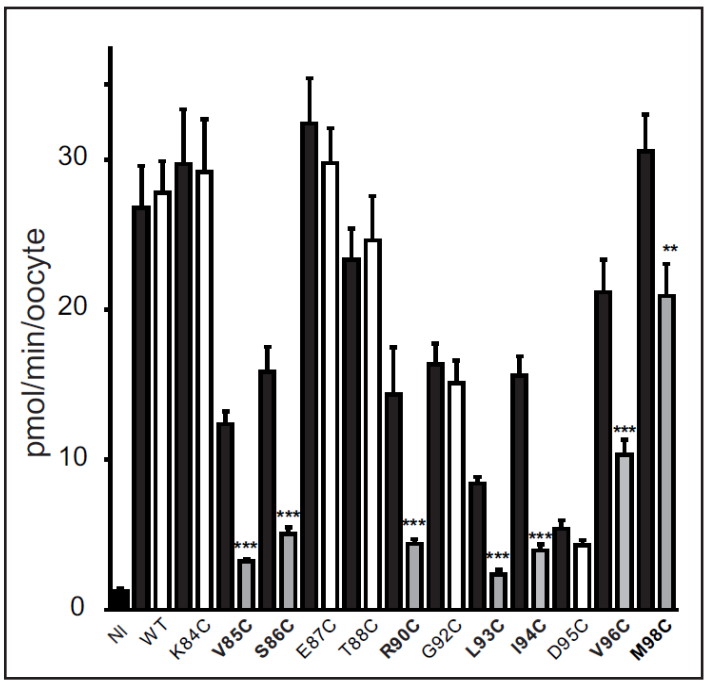

Fig. 2. Cysteine scanning of the 1st extracellular linker in PiT-1. Effect of thiol modification on ^{32}P uptake mediated by Cys mutants. Black bars: control group; open and grey bars: groups of oocytes expressing the same construct and preincubated in 1 mM MTSET for 5 min; grey bars: data sets that showed significant loss of transport activity after incubation. Data combined from two batches of oocytes. NI = non-injected control, WT = wild type XlPiT-1. For each mutant, the pooled data sets were compared using the Student's t-test for significance. ***: significantly different p< 0.0005; ** significantly different p< 0.005.

Results

Cysteine scanning mutagenesis in the first extracellular linker region of PiT-1

We substituted cysteines one by one at 18 sites in the predicted 1st extracellular linker of *Xenopus laevis* clone of PiT-1 (*Xl*PiT-1) (Fig. 1A). This region was chosen, based on previous mutagenesis studies that indicated that it contains functionally important residues [31, 37]. Moreover, hydrophobicity analysis predicted that this region was largely hydrophilic and should be accessible from the external medium (Fig. 1B). We expressed the mutant constructs in *Xenopus laevis* oocytes and assayed them for functional transport using ^{32}P. Oocytes for each mutant were divided into a control group incubated in 100Na alone and a group that was incubated for 5 min in 100Na together with the membrane impermeable methane thiosulfonate reagent, 2-(trimethylammonium)ethyl methane thiosulfonate bromide (MTSET) at 1 mM. After incubation, the oocytes were washed and the uptake assay was performed (see Materials and Methods). Fig. 2 shows the pooled data from two batches of oocytes from different donor animals. All constructs gave uptake levels that were at least 5-fold greater than that obtained from control, non-injected (NI) oocytes. For WT *Xl*PiT-1, preincubation in MTSET did not result in a significant change in ^{32}P uptake. This suggested that either none of the 17 native cysteines of *Xl*PiT-1 (Fig. 1A) was located in a functionally sensitive site, or if that were not the case, they were inaccessible from the external medium. We obtained the same result for mutants for which a Cys was substituted at 11 sites: Lys-84, Glu-87, Thr-88, Gly-92, Asp-95 (Fig. 2); at Lys-91 and from Asn-100 through to Leu-105 (data not shown)). In contrast, for mutants containing a Cys substituted at 7 sites (Val-85, Ser-86, Arg-90, Leu-93, Iso-94, Val-96, Met-98), the expressing oocytes showed a significant decrease in ^{32}P uptake after preincubation in MTSET (Fig. 2).

Determination of accessibility using electrophysiology

To better define the conditions under which the thiol modification took place and quantitate the accessibility of the substituted cysteines, we used the two-electrode voltage clamp (TEVC) to control the membrane potential during the modification reaction and assay the behavior of single oocytes. Fig. 3A shows pooled data for the dependence of P_i-induced current (I_P) on membrane potential (V) for the mutant V96C data before and after incubation in MTSET (1 mM for 3 min). This mutant showed an almost complete suppression

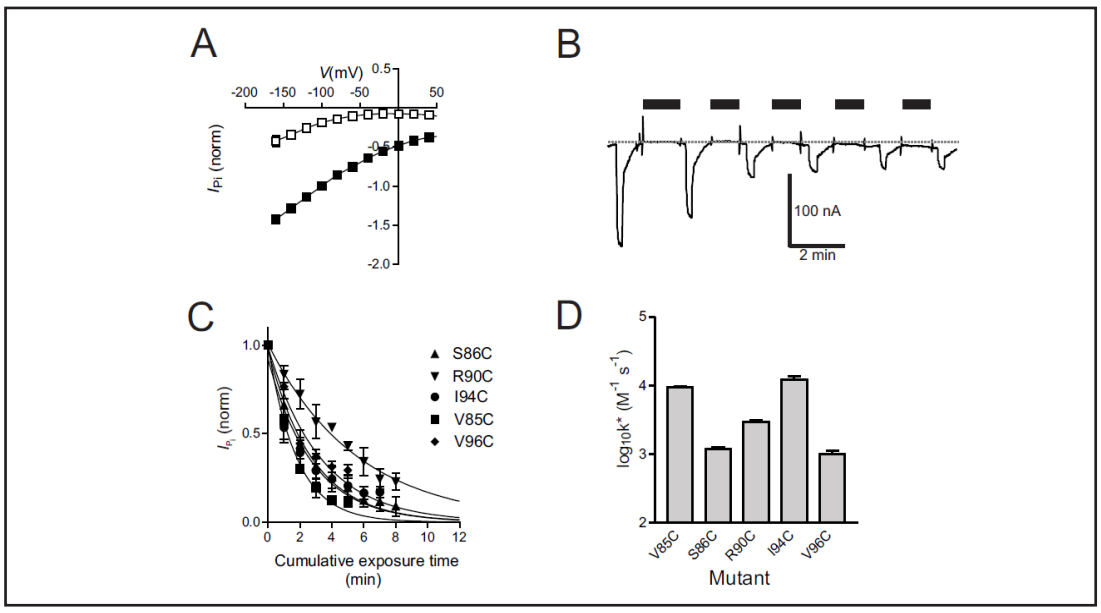

Fig. 3. Loss of transport activity during thiol modification depends on site of Cys-substitution.A) Electrophysiological recording from oocytes expressing the mutant V96C showing P_i-induced current (I_{P_i}) before (closed symbols) and after (open symbols) incubation in 1 mM MTSET for 5 min. Oocytes were voltage clamped at -50 mV during the incubation. Error bars smaller than symbol not shown. Data pooled from 4 oocytes and normalized to control I_{P_i} at -100 mV. B) Representative time course of I_{P_i} at -50 mV showing progressive loss of electrogenic activity after succeeding incubation periods in MTSET (5 μM) for an oocyte expressing mutant V96C. Bars represent period of incubation. Artefact spikes occur when continuous perfusion was switched off and MTSET solution added to recording chamber. Broken line represents reference holding current at start of experiment. C) Time dependence of loss of electrogenic activity for 5 mutants indicated. Each data set, pooled from 4 or more oocytes was normalized to the initial I_{P_i}. Continuous lines are fits using Eqn 2. The MTSET concentrations were (in μM): 0.5 (I94C); 1 (V85C, R90C); 5 (S86C, V96C). D) Effective 2nd order rate constant (k*) plotted logarithmically for each Cys-mutant. The constant was derived from exponential curve fits by dividing the exponent by the MTSET concentration used to perform the assay as indicated in C). Error bars are SEM reported by fit.

of I_{P_i}, whereas for the uptake assay under non-voltage clamp conditions, we observed only 50% inhibition (Fig. 2). We also confirmed that the Cys-modification was reversible: after treatment with MTSET a representative oocyte was removed from the recording chamber and incubated for 10 min in the reducing agent dithiothreitol DTT (10 mM). This resulted in 75% recovery of the original I_{P_i}-V response, which confirmed that altered transport activity was most likely a result of the Cys-modification (data not shown).

The Cys-modification reaction rate, used to estimate the accessibility of the cysteine, was determined by measuring the progressive change in I_{P_i} after repeated exposure of the oocyte to MTSET for 1 min intervals (see Materials and methods). Fig. 3B shows the response of a representative oocyte that expressed the mutant V96C with 10 μM MTSET applied for 1 min intervals. The oocyte remained voltage clamped at -50 mV throughout the assay. The normalized response plotted as a function of cumulative exposure time showed behavior that could be described by a single decaying exponential (Eqn 2). The exponential fitting procedure allowed us to estimate the effective 2nd order rate of Cys-modification (k^*) (Fig. 3C) according to a simplified model for Cys-modification [38]. The magnitude of this reaction rate may be interpreted as a measure of the accessibility of the cysteine from the extracellular milieu. For the 5 mutants that gave reliable electrogenic responses, we found that k^* varied according to the site of substitution (Fig. 3D).

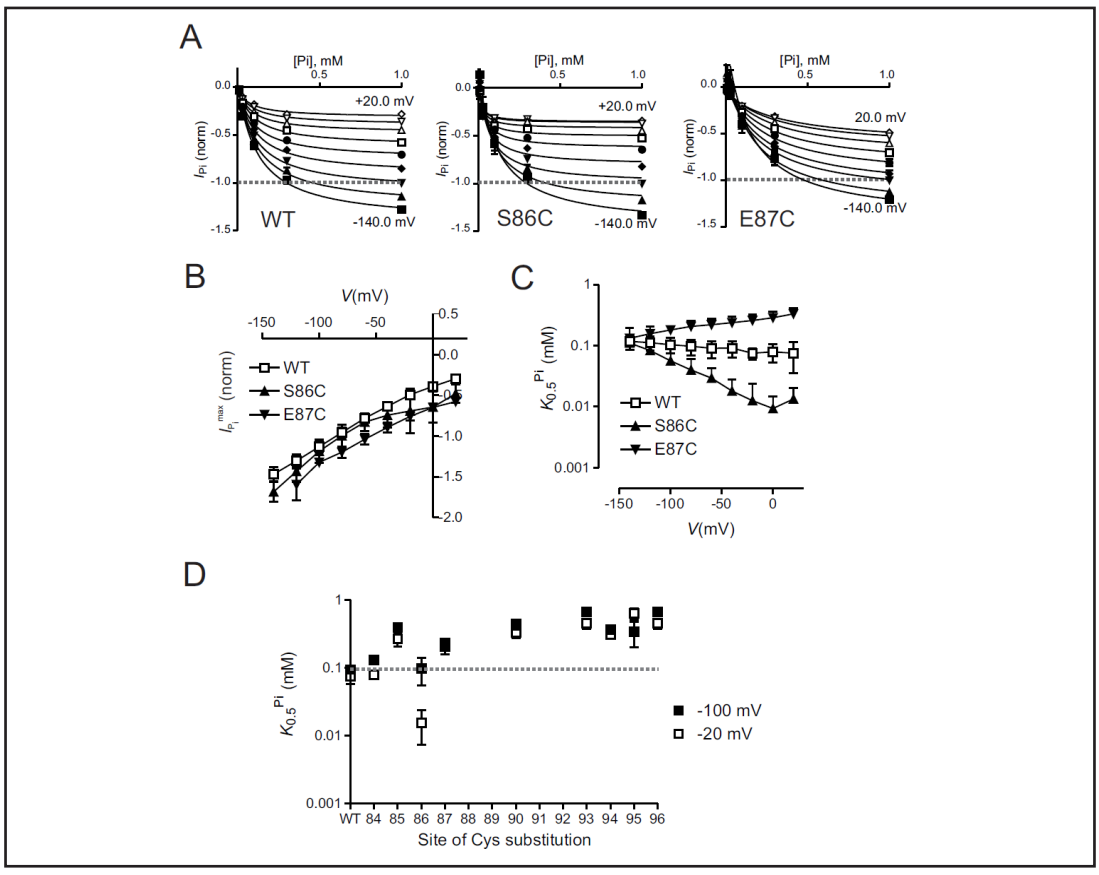

Fig. 4. P_i-activation for selected mutants determined by electrophysiology. A) Normalised P_i-activation data for WT (left panel) and mutants S86C (center panel) and E87C (right panel) for different membrane voltages from -140 to +20 mV. Continuous lines are fits using Eqn 1. Data for individual oocytes were normalized to the response at -100 mV, 1 mM P_i and pooled (n≥ 3). Dashed lines indicate normalizing value (-100 mV, 1 mM P_i). B) Maximum P_i-induced current (I_{max}^{Pi}) predicted from fits using Eqn 1, plotted as a function of membrane potential for WT (open squares), S86C (triangles) and E87C (inverted triangles). Data points are joined by lines for visualization only. Error bars represent SEM reported by fit to pooled normalized data. C) Apparent affinity constant for P_i ($K_{0.5}^{Pi}$) predicted from fits using Eqn 1, plotted logarithmically as a function of membrane potential for WT and S86C and E87C. Same symbols as in B). Error bars represent SEM reported by fit to pooled normalized data. D) Summary of $K_{0.5}^{Pi}$ data (plotted logarithmically) for all mutants tested in this study shown for two potentials: -100 mV (filled squares) and -20 mV (open squares). Dashed line indicates WT value at -100 mV.

Cys-mutagenesis alters substrate interactions

Cys-substitution was generally well tolerated with respect to basic transport function (Fig. 2), however we could not exclude the possibility that the Cys-substitution itself had altered the transport kinetics. To investigate this, we first performed a P_i-activation assay and determined the apparent affinity for P_i ($K_{0.5}^{Pi}$, Eqn 1) as a function of membrane potential for mutants that gave adequate electrogenic responses. Representative P_i-activation data two mutants (S86C and E87C) that gave contrasting behavior from the WT are shown in Fig. 4A for a range of potentials. The voltage dependence of I_{max}^{Pi} and $K_{0.5}^{Pi}$ predicted from the fits is shown in Fig. 4B, C respectively. Both mutants S86C and E87C showed a WT-like voltage dependence for the normalised I_{max}^{Pi} (Fig. 4B) with a characteristic curvilinear dependence on V as we have previously reported [19]. Uncertainties in the fit results arising from the incomplete saturation of the P_i-activation could easily explain the deviations observed. In contrast their $K_{0.5}^{Pi}$ dependence on V (Fig. 4C) both deviated from the relatively voltage-

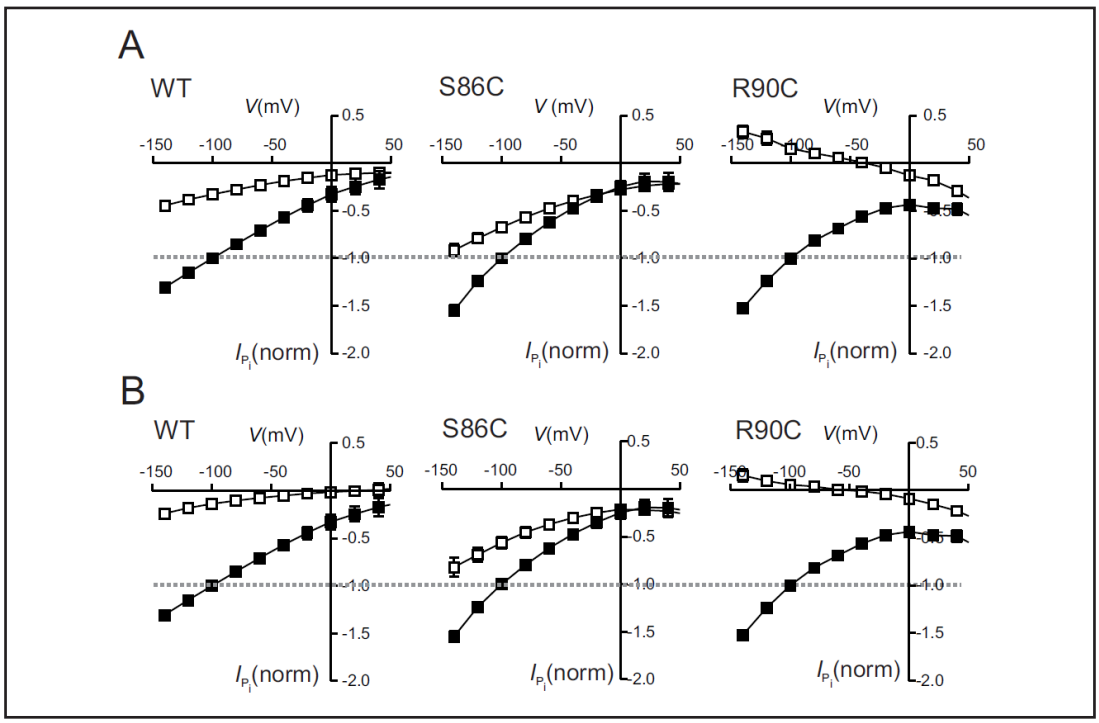

Fig. 5. Cysteine mutagenesis alters substrate selectivity for mutant S86C and R90C. A) Comparison of electrogenic response to 1mM P_i (filled squares) or 1 mM AsO_4 (open squares) (pH 7.4, 100 mM Na^+) for WT (left panel), S86C (centre panel) and R90C (right panel). In each panel, the data were normalized to the response to P_i (1 mM) at -100 mV. Dashed line is used to compare response at -100 mV, 1 mM P_i. Data pooled from 4 oocytes. B) Comparison of electrogenic response to P_i with 100 mM Na^+ (filled squares) substituted equimolarly with Li (open squares) for WT (left panel), S86C (centre panel) and R90C (right panel). In each panel, the data were normalized to the response to P_i (1 mM) and 100 mM Na^+ at -100 mV (same data set as in A)). Dashed line is used to compare response at -100 mV, 1 mM P_i and 100 mM Na^+. Data pooled from 4 oocytes.

insensitive WT characteristic at depolarizing potentials [19]. At V= 0 mV, $K_{0.5}^{P_i}$ for E87C was approximately 3-fold higher, whereas mutant S86C, which involved a conservative substitution, showed a significant decrease of ≈ 10-fold compared with the WT. At strong membrane hyperpolarization, the $K_{0.5}^{P_i}$ data for the mutants appeared to approach that of the WT (Fig. 4C). The effect of Cys substitution on $K_{0.5}^{P_i}$ for all mutants examined is summarised in Fig. 4D, which shows $K_{0.5}^{P_i}$ at -100 mV and -20 mV. With the exception of S86C and K84C, all mutants showed a reduced apparent affinity for P_i compared with the WT at these potentials.

Next we compared the behavior of two mutants (S86C and R90C) with respect to substrate specificity and voltage dependence. Two features were readily apparent. First, both S86C and R90C showed a more obvious curvilinear *I-V* behavior compared with the WT for P_i activation at 1 mM P_i. Second, we and others have reported that substitution of arsenate for P_i also results in measurable transport activity by SLC20 proteins [19, 28]. Using 1 mM AsO_4 (pH 7.4) as the activating substrate added to 100Na resulted in a ≈60% reduction in electrogenic response for the WT PiT-1 (Fig. 5A, left panel), whereas for mutant S86C the reduction was only 25% (at -100 mV) (Fig. 5A, centre panel). In contrast, mutant R90C, which displayed a voltage dependence for I_{P_i} similar to S86C, showed a reversal of the AsO_4-induced current for hyperpolarizing potentials at approximately -50 mV (Fig. 5A, right *panel)*.

Finally, we compared the behavior of these mutants when Li^+ replaced Na^+ as the driving cation. The former has also been previously reported to act as a driving cation for

SLC20 proteins [6, 29, 42]. When Li^+ was substituted, equimolarly for Na^+, the WT showed a significantly reduced electrogenic response to P_i (Fig. 5B, left panel)), whereas for S86C the cation substitution resulted in a 25% reduction (at -100 mV) (Fig. 5B, centre panel). Moreover, R90C expressing oocytes showed a similar behavior to that observed for arsenate substitution, whereby I_{P_i} reversed direction at approximately -50 mV (Fig. 5B, right panel).

Discussion

The aims of this study were twofold: (i) to investigate the topology in a specific region of the PiT-1 protein predicted to be an external linker by means of the cysteine scanning accessibility method (SCAM) and (ii) to identify functionally important sites resulting from Cys-substitution and subsequent thiol modification. SCAM has previously proven useful when applied to members of the type II Na^+/P_i cotransporter (SLC34 family) (for review see [3]). An important caveat for its successful application is that only the substituted Cys should be the target of the thiol reaction. *Xl*PiT-1 contains 17 native Cys (Fig. 1) and although the WT protein showed no apparent change in transport function when incubated in MTSET, we cannot exclude the possibility that for the mutants, the Cys-mutagenesis may have resulted in a unique conformational change that exposed one of the native Cys to the extracellular medium (e.g. [43]). It was reported that a Cys-less PiT-1 has been synthesized for topology investigations in the context of identifying the virus receptor motif [34], however in that study the protein was expressed in a fibroblast cell line and no assays were performed to confirm functional transport of P_i. Given the lack of altered transport function for the WT and that for the mutants described in this study the reduction was site-dependent, we tentatively assume that only the substituted Cys were involved. Nevertheless, future structure-function studies on PiT-1 should involve removal of native Cys to confirm the validity of the present findings.

The choice of the 1st extracellular linker region in PiT-1 was based on a previous report, that mutagenesis at two sites in this region of the human PiT-2 (Glu-68, corresponding to Glu-87 in *Xl*PiT-1; and Asp-76 corresponding to Asp-95 in *Xl*PiT-1) had a significant effect on PiT-2 transport function when the mutants were expressed in *Xenopus* oocytes [31]. We found that Cys-substitution at one of the two sites identified by Bøttger and Pedersen [31] (mutant E87C), was well tolerated and exhibited comparable uptake to the WT although its apparent P_i affinity was reduced compared with the WT at depolarizing potentials (Fig. 4C). In contrast, substitution at the other site (mutant D95C) resulted in significantly diminished uptake (Fig. 2), in agreement with the PiT-2 study in which the native Glu was replaced by a Gln [31]. Without a means to quantitate the amount of protein expressed at the membrane, we are unable to conclude whether the reduced transport function that we observed for D95C resulted from a concomitantly smaller transport rate or membrane expression level. From the P_i-activation data, the reduced apparent affinity for P_i (Fig. 4D) could, in part, account for the observed behavior. What is certain is that for both these mutants there was insignificant change in uptake level after exposure to MTSET (Fig. 2). This suggested that these sites are either not readily accessible to the external medium or, if accessible, the Cys-modification did not alter the ability of the protein to catalyse P_i transport. In contrast, we found that Cys substitution at the neighboring site (Ser-86) was, like Glu-87, well tolerated (mutant S86C), but MTSET incubation resulted in significant loss of transport activity. Moreover, Cys-substitution at the sites neighboring Asp-95 (mutants I94C and V96C) was also well tolerated and showed control uptake levels approximately 50% of the WT. However, MTSET incubation led to significant loss of activity, which indicated that their transport function was severely compromised and, moreover, confirmed the accessibility of Cys to the external milieu at sites 94 and 96.

Our initial SCAM assay by means of ^{32}P uptake identified 6 sites for which MTSET exposure resulted in a loss of transport function and we turned to electrophysiological assays to investigate some features in more detail, where we could readily observe the thiol

modification reaction in real time and control the transport conditions. Interestingly, when the uptake results were compared with the results of the same construct under voltage clamp, we generally observed a larger reduction in transport activity for individually voltage-clamped oocytes. In addition to the statistical variation inherent in the uptake assays, this discrepancy may arise because we performed the uptake assays under non-voltage clamp conditions. If the accessibility of the Cys were influenced by the membrane potential, this could affect the proportion of modified transporters.

The TEVC assay allowed us to estimate the effective 2nd order rate constant (k*) for 5 mutants that gave reproducible electrogenic responses to P_i (Fig. 3D). The estimates of k* were in the same range as we have previously reported for a comparable assay performed on the SLC34A1 protein (NaPi-IIa) [44]. For *Xl*PiT-1, the assay revealed that sites Val-85 and Iso-94 showed significantly higher modification rate compared with the others, which suggested that these sites were more exposed to the aqueous environment. That their Cys-modification led to a compromised transport function further suggests that they may be close to or part of the substrate binding site(s). In summary, our SCAM findings suggest that the topology of this linker region is most likely not simply an "external" loop that is uniformly exposed to the extracellular milieu, but may indeed form part of a hydrophilic pore region in which substrates might be expected to interact and bind to the specific sites during the transport cycle. Additional experiments to test this hypothesis should include performing the Cys-modification assay at different holding potentials and in the complete absence of substrate or in the presence of Na^+ and P_i. These manipulations would be expected to place the transporters in different conformations that would alter the accessibility of the substituted Cys if they were close to the substrate binding sites.

Further evidence in support of this speculation in the present study came from electrophysiological assays applied to two mutants that showed a significant loss of activity after thiol modification (S86C and R90C). Mutant S86C, which involved a conservative Ser to Cys substitution showed the same apparent affinity for P_i as the WT at hyperpolarizing potentials, however its $K_{0.5}^{P_i}$ decreased by ≈10-fold at V=0 (Fig. 4C). This suggested that the residue at this site was a critical determinant of voltage dependent substrate interactions with PiT-1. The Ser-Cys substitution at site 86 also increased the relative response to As, which further suggested that the mutagenesis had altered substrate coordination (Fig. 5A). Moreover, substitution of Na^+ by Li^+ resulted in a significantly increased electrogenic activity compared with the WT (Fig. 5B).

In contrast, removal of charge at site 90 (mutant R90C), increased the voltage dependency of I_{P_i} (like S86C), but this mutant could neither support elecrogenic cotransport by As with Na^+ as the driving cation nor by P_i when Li^+ equimolarly replaced Na^+. These findings indicated that the charge at this site was critical for substrate discrimination, although we observed only a small increase in $K_{0.5}^{P_i}$ for the R90C mutant compared with the WT (Fig. 4D). It was also noteworthy that when Cys-90 was presumably modified by MTSET, electrogenic cotransport function was fully suppressed. MTSET is positively charged, but when covalently bound to a Cys, results in a bulkier side chain (122 Å^3 versus 173 Å^3) [45], which further underscores the critical role this site plays in substrate coordination. Mutant R90C also showed a unique electrogenic behavior for both substrate replacement experiments: I_{P_i} showed a reversed with an apparent outward current for hyperpolarizing potentials (Fig. 5B). This behavior was not observed in non-injected oocytes (data not shown) and suggests that the substrates do indeed interact with the protein, but the full cotransport cycle with net inward charge movement does not occur. This electrogenic response might be evidence of an uncoupled leak current that is suppressed during the cotransport cycle. Analogous behavior has been reported for SLC34A1 proteins for which an uncoupled leak can be detected using the P_i-transporter inhibitor phosphonoformic acid [46], the sodium-coupled glucose cotransporter SGLT1 for which pflorizin is known to block a protein-associated uncoupled leak [47, 48] and other cation-coupled cotransporters. Presently there is no PiT-specific inhibitor available to investigate this phenomenon further in the SLC20 family.

Conclusions

We have established that an extracellular linker in *Xl*PiT-1 is accessible to the external medium and thereby confirmed previous topological predictions for the SLC20 family. Moreover, we have shown that this region contains amino acids that are critical for the unique transport kinetics of SLC20 proteins-in particular the apparent affinity for P_i and the cation and P_i/As discrimination. This information will pave the way for further studies to identify functionally important regions of the SLC20 proteins and may also be used to define sites for drug targeting, particularly as no specific inhibitor of SLC20 proteins is currently available.

Acknowledgements

We thank Eva Hänsenberger for the oocytes preparation, Dr Leila Virkki for guidance with preparation of the mutants and Dr Anne-Kristine Meinild for helpful comments on the manuscript. This work was supported financially by the Swiss National Science Foundation and Gebert-Rüf Stiftung (www.grstiftung.ch) (to HM).

References

1 Forster I, Hernando N, Sorribas V, Werner A: Phosphate transporters in renal, gastrointestinal, and other tissues. Adv Chronic Kidney Dis 2011;18:63-76.
2 Forster IC, Hernando N, Biber J, Murer H: Proximal tubular handling of phosphate: A molecular perspective. Kidney Int 2006;70:1548-1559.
3 Forster IC, Hernando N, Biber J, Murer H: Phosphate transport kinetics and structure-function relationships of SLC34 and SLC20 proteins. Curr Top Membr 2012;70:313-356.
4 Miyamoto K, Haito-Sugino S, Kuwahara S, Ohi A, Nomura K, Ito M, Kuwahata M, Kido S, Tatsumi S, Kaneko I, Segawa H: Sodium-dependent phosphate cotransporters: Lessons from gene knockout and mutation studies. J Pharm Sci 2011;100:3719-3730.
5 Kavanaugh MP, Miller DG, Zhang W, Law W, Kozak SL, Kabat D, Miller AD: Cell-surface receptors for gibbon ape leukemia virus and amphotropic murine retrovirus are inducible sodium-dependent phosphate symporters. Proc Natl Acad Sci U S A 1994;91:7071-7075.
6 Wilson CA, Eiden MV, Anderson WB, Lehel C, Olah Z: The dual-function hamster receptor for amphotropic murine leukemia virus (MuLV), 10a1 MuLV, and gibbon ape leukemia virus is a phosphate symporter. J Virol 1995;69:534-537.
7 Olah Z, Lehel C, Anderson WB, Eiden MV, Wilson CA: The cellular receptor for gibbon ape leukemia virus is a novel high affinity sodium-dependent phosphate transporter. J Biol Chem 1994;269:25426-25431.
8 Nishimura M, Naito S: Tissue-specific mrna expression profiles of human solute carrier transporter superfamilies. Drug Metab Pharmacokinet 2008;23:22-44.
9 Zoidis E, Ghirlanda-Keller C, Gosteli-Peter M, Zapf J, Schmid C: Regulation of phosphate (Pi) transport and NaPi-III transporter (PiT-1) mrna in rat osteoblasts. J Endocrinol 2004;181:531-540.
10 Caverzasio J, Bonjour JP: Characteristics and regulation of Pi transport in osteogenic cells for bone metabolism. Kidney Int 1996;49:975-980.
11 Suzuki A, Ghayor C, Guicheux J, Magne D, Quillard S, Kakita A, Ono Y, Miura Y, Oiso Y, Itoh M, Caverzasio J: Enhanced expression of the inorganic phosphate transporter PiT-1 is involved in BMP-2-induced matrix mineralization in osteoblast-like cells. J Bone Miner Res 2006;21:674-683.
12 Villa-Bellosta R: On the role of the type III phosphate transporters in vascular calcification. Bone 2012;51:828; author reply 829.
13 Lau WL, Festing MH, Giachelli CM: Phosphate and vascular calcification: Emerging role of the sodium-dependent phosphate co-transporter PiT-1. Thromb Haemost 2010;104:464-470.
14 Jono S, McKee MD, Murry CE, Shioi A, Nishizawa Y, Mori K, Morii H, Giachelli CM: Phosphate regulation of vascular smooth muscle cell calcification. Circ Res 2000;87:E10-17.

15 Li X, Yang HY, Giachelli CM: Role of the sodium-dependent phosphate cotransporter, PiT-1, in vascular smooth muscle cell calcification. Circ Res 2006;98:905-912.
16 Mizobuchi M, Ogata H, Hatamura I, Koiwa F, Saji F, Shiizaki K, Negi S, Kinugasa E, Ooshima A, Koshikawa S, Akizawa T: Up-regulation of Cbfa1 and PiT-1 in calcified artery of uraemic rats with severe hyperphosphataemia and secondary hyperparathyroidism. Nephrol Dial Transplant 2006;21:911-916.
17 Shobeiri N, Adams MA, Holden RM: Phosphate: An old bone molecule but new cardiovascular risk factor. Br J Clin Pharmacol 2013; doi: 10.1111/bcp.12117.
18 Salaun C, Leroy C, Rousseau A, Boitez V, Beck L, Friedlander G: Identification of a novel transport-independent function of PiT1/SLC20A1 in the regulation of tnf-induced apoptosis. J Biol Chem 2010;285:34408-34418.
19 Ravera S, Virkki LV, Murer H, Forster IC: Deciphering pit transport kinetics and substrate specificity using electrophysiology and flux measurements. Am J Physiol Cell Physiol 2007;293:C606-620.
20 Moe OW: PiT-2 coming out of the pits. Am J Physiol Renal Physiol 2009;296:F689-690.
21 Villa-Bellosta R, Sorribas V: Compensatory regulation of the sodium/phosphate cotransporters NaPi-IIc (SCL34A3) and PiT-2 (SLC20A2) during Pi deprivation and acidosis. Pflugers Arch 2010;459:499-508.
22 Wang C, Li Y, Shi L, Ren J, Patti M, Wang T, de Oliveira JR, Sobrido MJ, Quintans B, Baquero M, Cui X, Zhang XY, Wang L, Xu H, Wang J, Yao J, Dai X, Liu J, Zhang L, Ma H, Gao Y, Ma X, Feng S, Liu M, Wang QK, Forster IC, Zhang X, Liu JY: Mutations in SLC20A2 link familial idiopathic basal ganglia calcification with phosphate homeostasis. Nat Genet 2012;44:254-256.
23 da Silva RJ, Pereira IC, Oliveira JR: Analysis of gene expression pattern and neuroanatomical correlates for SLC20A2 (PiT-2) shows a molecular network with potential impact in idiopathic basal ganglia calcification ("Fahr's disease"). J Mol Neurosci 2013;50:280-283.
24 Saliba KJ, Martin RE, Broer A, Henry RI, McCarthy CS, Downie MJ, Allen RJ, Mullin KA, McFadden GI, Broer S, Kirk K: Sodium-dependent uptake of inorganic phosphate by the intracellular malaria parasite. Nature 2006;443:582-585.
25 Schaffhauser DF, Patti M, Goda T, Miyahara Y, Forster IC, Dittrich PS: An integrated field-effect microdevice for monitoring membrane transport in xenopus laevis oocytes via lateral proton diffusion. PLoS One 2012;7:e39238.
26 Bottger P, Hede SE, Grunnet M, Hoyer B, Klaerke DA, Pedersen L: Characterization of transport mechanisms and determinants critical for Na^+-dependent Pi symport of the PiT family paralogs human PiT1 and PiT2. Am J Physiol Cell Physiol 2006;291:C1377-1387.
27 Villa-Bellosta R, Levi M, Sorribas V: Vascular smooth muscle cell calcification and SLC20 inorganic phosphate transporters: Effects of PDGF, TNF-α, and Pi. Pflugers Arch 2009;458:1151-1161.
28 Villa-Bellosta R, Sorribas V: Arsenate transport by sodium/phosphate cotransporter type IIb. Toxicol Appl Pharmacol 2010;247:36-40.
29 Bottger P, Pedersen L: Two highly conserved glutamate residues critical for type III sodium-dependent phosphate transport revealed by uncoupling transport function from retroviral receptor function. J Biol Chem 2002;277:42741-42747.
30 Bottger P, Pedersen L: The central half of PiT2 is not required for its function as a retroviral receptor. J Virol 2004;78:9564-9567.
31 Bottger P, Pedersen L: Evolutionary and experimental analyses of inorganic phosphate transporter PiT family reveals two related signature sequences harboring highly conserved aspartic acids critical for sodium-dependent phosphate transport function of human pit2. FEBS J 2005;272:3060-3074.
32 Bottger P, Pedersen L: Mapping of the minimal inorganic phosphate transporting unit of human PiT2 suggests a structure universal to PiT-related proteins from all kingdoms of life. BMC Biochem 2011;12:21.
33 Farrell K, Russ JL, Murthy RK, Eiden MV: Reassessing the role of region A in PiT1-mediated viral entry. J Virol 2002;76:7683-7693.
34 Farrell KB, Tusnady GE, Eiden MV: New structural arrangement of the extracellular regions of the phosphate transporter SLC20A1, the receptor for gibbon ape leukemia virus. J Biol Chem 2009;284:29979-29987.
35 Salaun C, Rodrigues P, Heard JM: Transmembrane topology of PiT-2, a phosphate transporter-retrovirus receptor. J Virol 2001;75:5584-5592.

36 Feldman SA, Farrell KB, Murthy RK, Russ JL, Eiden MV: Identification of an extracellular domain within the human PiT2 receptor that is required for amphotropic murine leukemia virus binding. J Virol 2004;78:595-602.
37 Bottger P, Hede SE, Grunnet M, Hoyer B, Klaerke DA, Pedersen L: Characterization of transport mechanisms and determinants critical for Na^+-dependent Pi symport of the PiT-family paralogs, human PiT1 and PiT2. Am J Physiol Cell Physiol 2006;291:C1377-1387.
38 Karlin A, Akabas MH: Substituted-cysteine accessibility method. Methods Enzymol 1998;293:123-145.
39 Virkki LV, Forster IC, Hernando N, Biber J, Murer H: Functional characterization of two naturally occurring mutations in the human sodium-phosphate cotransporter type IIa. J Bone Miner Res 2003;18:2135-2141.
40 Virkki LV, Murer H, Forster IC: Voltage clamp fluorometric measurements on a type II Na^+-coupled Pi cotransporter: Shedding light on substrate binding order. J Gen Physiol 2006;127:539-555.
41 Forster I, Hernando N, Biber J, Murer H: The voltage dependence of a cloned mammalian renal type II Na^+/Pi cotransporter (NaPi-2). J Gen Physiol 1998;112:1-18.
42 Villa-Bellosta R, Bogaert YE, Levi M, Sorribas V: Characterization of phosphate transport in rat vascular smooth muscle cells: Implications for vascular calcification. Arterioscler Thromb Vasc Biol 2007;27:1030-1036.
43 Kamdar G, Penado KM, Rudnick G, Stephan MM: Functional role of critical stripe residues in transmembrane span 7 of the serotonin transporter. Effects of Na^+, Li^+, and methanethiosulfonate reagents. J Biol Chem 2001;276:4038-4045.
44 Ehnes C, Forster IC, Kohler K, Bacconi A, Stange G, Biber J, Murer H: Structure-function relations of the first and fourth predicted extracellular linkers of the type IIa Na^+/Pi cotransporter: I. Cysteine scanning mutagenesis. J Gen Physiol 2004;124:475-488.
45 Xu Y, Kakhniashvili DA, Gremse DA, Wood DO, Mayor JA, Walters DE, Kaplan RS: The yeast mitochondrial citrate transport protein. Probing the roles of cysteines, Arg(181), and Arg(189) in transporter function. J Biol Chem 2000;275:7117-7124.
46 Andrini O, Ghezzi C, Murer H, Forster IC: The leak mode of type II Na^+/-Pi cotransporters. Channels (Austin) 2008;2:346-357.
47 Longpre JP, Gagnon DG, Coady MJ, Lapointe JY: The actual ionic nature of the leak current through the Na^+/glucose cotransporter SGLT1. Biophys J 2010;98:231-239.
48 Umbach JA, Coady MJ, Wright EM: Intestinal Na^+/glucose cotransporter expressed in xenopus oocytes is electrogenic. Biophys J 1990;57:1217-1224.
49 Gasteiger E, Hoogland C, Gattiker A, Duvaud S, Wilkins MR, Appel RD, Bairoch A: in Walker JM (ed): Protein Identification and Analysis Tools on the ExPASy Server. Humana Press, Totowa, New Jersey, Springer, 2005, pp. 571-607.